HOW SAILS GENERATE FORCES

I. M. Viola, University of Edinburgh, UK, i.m.viola@ed.ac.uk.
A. Arredondo-Galeana, University of Edinburgh, UK, a.arredondo@ed.ac.uk.
G. Pisetta, University of Edinburgh, UK, gabriele.pisetta@ed.ac.uk.

We propose a new paradigm of the aerodynamics of sails that reconciles our understanding of the force generation mechanisms of both upwind and downwind sails, and that is applicable to both attached and separated flow conditions. Sail experience significant flow separation. Even when the flow appears to be attached, this is sometimes only in the time averaged sense. In these conditions, the underlining assumptions of thin airfoil theory and lifting line theory are violated. There is therefore a need to develop an intuitive understanding of the force generation mechanisms that does not rely on these assumptions. This paper aims to address this issue by proposing a new paradigm based on the impulse theory. The force generation mechanism can be intuitively associated with the vorticity field, which can be gathered with computational fluid dynamics or particle image velocimetry. This paradigm intuitively reconciles key results of traditional wing aerodynamics, and provides sail designers a measurable objective to modify a sail shape also in separated flow conditions. It will hopefully underpin both a deeper understanding of sail aerodynamics and the development of low order models for new design tools.

1 Background

The origin of lift is one of the most fundamental questions in sail aerodynamics and one of the most difficult to address. Despite its critical significance, there is not yet a satisfactory explanation on the origin of lift for the layperson [1]. One of the major efforts of disseminating fundamental fluid mechanics knowledge to the sailing community was that of Arvel Gentry, who passed away two years ago and to whom this article is dedicated. In 1973, Gentry, who worked for Douglas Aircraft Company, wrote on Sail Magazine a series of 11 articles [2]. He explained sail aerodynamics in terms of circulation and argued, for example, that there was not a Venturi effect between sails. The theory was so counterintuitive that most people refused to accept it. The Venturi effect is still used in many sailing schools to explain (incorrectly) the interaction between sails. Soon after Gentry's article, Peter Barrett, who was the Vice President of North Sails, wrote on Yacht Racing: *"I am willing to state categorically that* [Gentry's] *future articles will do little, if anything, to improve directly the performances of both sailboats and sailors."* It took almost 20 years before Gentry's article changed the common understanding of sail aerodynamics. In 1990, Tom Whidden, the new President of North Sails, together with Michael Levitt published the seminal book The Art and Science of Sails, which completely endorsed Gentry's articles. Five years after this book was published, in 1995, Doug Logan (Consulting Editor to Sailing World) wrote: *"The foundation of sailing have been demolished, quietly and completely?* [3].

Gentry explained the concept of circulation that was developed independently in the early 1900s by Lancaster [4] in the UK, Kutta [5] in Germany and Zhukovsky [6] (sometimes Joukovsky or Joukowsky or Joukowski) in Russia. By the 1970s, the concept of circulation was widely adopted in aeronautics and by the academic community involved with America's Cup yacht design (e.g. Jerome Milgram [7]), but it was still ignored by the wider sailing community.

In summary, a solid body immersed in a moving fluid results necessarily in fluid rotation (Ω), whose measure is the vorticity ($\omega = 2\Omega$); and the integral of the vorticity over a volume is the circulation (Γ). A solid body within a moving fluid must be immersed in a layer of vorticity; if the overall integral of vorticity is not null, then there is bound circulation around the body. The circulation can be described as the strength of a point vortex that induces a tangential velocity inversely proportional to the distance from its centre. The flow around a sail can be considered as the vectorial sum of the free stream velocity and the induced velocity of the sail vortex. Hence, the simplest model of a sail is a point vortex with circulation equal to the integral of all of the vorticity in its boundary layer.

The lift force due to the combination of the free stream velocity and the velocity induced by the sail vortex can be easily computed by using a convenient solid surface of arbitrarily radius a around the vortex (for example, this can be included in the complex potential as a doublet). Compute the velocity on the cylinder surface as the vectorial sum of the free stream velocity and the vortex-induced velocity, and use the Bernoulli equation to compute the pressure distribution around the cylinder. The pressure integral in the lift direction on the cylinder surface is the lift. The result is $L = -\rho U \Gamma$, which is the Kutta-Joukowski theorem. This theorem shows that the lift only depends on air density ρ, the free stream velocity U and the sail circulation Γ. An equivalent formulation

was derived by Filon [8] for the drag: $D = \rho U Q_\psi$, where Q_ψ is the net flow rate into the wake of the vector potential derived by Helmholtz decomposition. Unfortunately, however, Q_ψ cannot be directly measured [9].

The force production mechanisms is explained in terms of bound circulation in virtually all of the sail aerodynamics books (e.g. Whidden and Levitt [10], Larsson and Eliasson [11], Claughton et al. [12], Fossati [13], van Ossanen [14], etc.). As discussed in the following, this model is fairly accurate for upwind sails where the vorticity is confined within the sail boundary layer. Moreover, it allows explaining intuitively the interaction between the two sails and why Venturi effect does not apply [15, 16]. On the other hand, when flow separation occurs, we are left with very little explanations. What is most remarkable is that flow separation occurs in most of the conditions on a yacht sail and, yet, we do not have a conceptual model to account for its effect.

2 Sail Aerodynamics

2.1 Sail Aerodynamics in the Sailing Literature

Except for the mainsail, sails have a sharp leading edge and thus there is only one angle of attack, namely the ideal angle of attack, where the onset flow is tangent to the leading edge and an attached boundary layer develops on both sides of the sail. At any other lower angle of attack, the leading edge of the sail collapses, whilst at any higher angle of attack the flow separates. Flow separation is often not detected because it could be confined in a small region near the leading edge. When flow separation occurs, vorticity is shed downstream and rolls up into vortices, which might then roll along the sail or be shed away [17, 18]. The rolling of these vortices along the sail results, in a time averaged sense, in flow reattachment and in a recirculation region near the leading edge that is known as leading-edge separation bubble [19–27]. The bubble, which is typically shorter than 10% of the sail chord, can occur both on upwind [28–31] and on downwind sails [32,33].

On downwind sails, because the flow is strongly tridimensional [17, 34], the circulation shed by the shear layer might roll up into a leading edge vortex stably attached to the leading edge [17, 18]. The stability of leading edge vortices is the objective of several recent studies [35–39] and it is not yet clear if a stable vortex can exist on full-scale sails [40]. In addition, significant trailing edge separation always occurs on downwind sails [29] and its effect is poorly understood. In his seminal review, Milgram [41] stated that "for offwind sailing, flow separation is almost always large enough to significantly influence the lift, so experimental data are required to construct a mathematical model for it."

The fraction of sail area where the flow is separated increases by trimming in the sail and, in light wind conditions, the trim maximising the driving force is largely separated [42]. For example, the mainsail is largely separated in upwind, light wind conditions. If the optimal sail shape presents significant flow separation, then it is very difficult to intuitively identify how to improve a sail design. In fact, it is not possible to anticipate how the aerodynamic forces would vary between two sail shapes with significant flow separation. Paradoxically, while the most adopted explanation for the generation of lift force relies on the flow to be attached, the flow around sails is dominated by separated flow.

2.2 Sail Aerodynamics in the Fluid Mechanics Literature

Firstly, it must be clarified that the sail aerodynamics intended here is not what is called *sail aerodynamics* in the fluid mechanics literature, that is a flexible foil anchored at the edges. This is a canonical problem that was pioneered by Cisotti [43] and then followed by Voelz [44], Thwaites [45], Dugan [46], Smith & Shyy [47], etc. and also extended to the three dimensional problem of a flexible membrane [48–52]. Conversely, modern sails have sufficient tension in the structure that they behave as rigid wings, but the aerodynamics is characterised by the sharp leading edge.

To understand the underlying fluid mechanics of yacht sails it is useful to simplify their geometries to the essential features that explain the key observed phenomena. The force production mechanisms of yacht sails is that of low-aspect-ratio, swept, twisted, cambered plate. In fact, the key force production mechanisms of steadily translating, bidimensional, flat plates at incidence [53–56] is the same as that of yacht sails. The sharp leading edge of the plate and of the sail leads to similar separated flow fields at those angles of attack where a foil with a curved leading edge would experience an attached boundary layer. Hence, this flow condition is adopted in this paper to elaborate the proposed paradigm for yacht sails. For a list of flat plate studies, interested readers can find a useful table in Afgan et al. [57]. The effect of curvature [46, 58–60] can be considered as an increase of the effective angle of attack. Studies on highly-cambered circular arcs [61–65] allows to isolate the underlying differences between flatter upwind sails and deeper downwind sails. The favourable pressure gradient upstream of the maximum camber on curved plates promotes reattachment and the establishment of an attached boundary layer, which is unlikely on a flat plate. On the other hand, on the rear of a cambered plate, the adverse pressure gradient promotes trailing edge separation. For example, Suoppez et al. [32, 33] investigated on a circular arc how the leading edge bubble affects trailing edge separation, which is a phenomenon that occurs on cambered plates and not on flat plates. More studies on this subject are currently ongoing by the same authors.

The tridimensional effects are significant on sails because of their low aspect ratio. Whilst high aspect ratio wings have been largely investigated due to their significance in aeronautics and turbomachinery, low aspect ratio wings have received

comparatively less attention. However, due to the fast growing interest in small aerial vehicles, where the optimum aspect ratio of the wing is significantly lower than that of large aircrafts, research in this area has significantly increased in recent years. Interested readers on the effect of aspect ratio on the aerodynamics of flat plates can consider the rich literature surveys in Taira and Colonius [66], Lee et al. [67], and DeVoria and Mohseni [68]. Similarly, for the effect of sweep angle, consider the literature survey of Huang et al. [69]. The main effect of the low aspect ratio is to enable spanwise convection of vorticity, which, for example, can enable a stable leading edge vortex. Finally, it is instructive to note that the effect of sail twist is the same as that of a shear in the onset flow, and that the twist does not change the lift slope with the angle of attack [70].

3 Aim and Organisation of the Paper

The aim of this paper is to propose a new paradigm for the force production of yacht sails. This is based on well understood fluid mechanics principles, which, however, are not commonly applied to yacht sails. This is the vorticity-moment theory, or impulse theory, that describes the forces on a flow-immersed body as the result of the vortex flow in the whole flow field. The advantage of this approach is that it allows an intuitive rationale for how both lift and drag forces are generated in both attached and separated flow conditions. More specifically, it predicts the force contribution of any element of vorticity in the fluid, both in steady and unsteady conditions, both for rigid and flexible bodies. For example, we will show how the vorticity in different regions of separated flow contributes to the forces on the sail. Hence, it allows interpreting the force differences between two flow conditions with separated flow. This can guide sail designers to identify the optimum sail shape and to identify desirable and undesirable flow features in the fluid.

This vorticity-based approach is equivalent to the most common pressure-friction approach. However, while knowledge of the surface pressure on the sail allows the identification of the areas of the sail that most contribute to driving force [30], the pressure in the flow field does not provide any direct information of its effect of the sail. For example, a vortex on the suction side of the sail is typically assumed to contribute to lower the surface pressure and thus to lead to lift enhancement. However, the presence of a low pressure in the centre of the vortex does not necessarily result in a low pressure on the sail surface. In fact, we will show in Section 4 that the force on the sail due to that vortex depends on the sign of its circulation and on its velocity. Some vortices in the separated flow region provide a positive contribution to the lift and decrease the drag, while others decrease the lift and increase the drag.

The impulse theory is an equivalent formulation to the Navier-Stokes equations and, therefore, could be written in a formulation appropriate for numerical modelling (e.g. discrete vortex methods [71]). However, in this paper we do not consider these numerical methods and we focus on how this theory can be used to interpret the observed flow field. Interpreting the force generation mechanisms can, in turn, underpin low-order models to predict the forces [72–75]. Hence, whilst the proposed paradigm is not presented here as a predictive model per se (even if it could be), it is suggested that it can be used to develop low order models for sails experiencing separated flow, that are currently unavailable.

The rest of the paper is organised as follows. In Sec. 4 we critically review some key results of the impulse theory for bidimensional (2D) and tridimensional (3D) plates. We show how these results provide a physical interpretation of the forces exerted on the sail by vortex pairs in 2D (Sec. 4.1) and vortex rings in 3D (Sec. 4.2), and how they reconcile with thin airfoil theory and lifting line theory. In Sec. 5 we provide our own analysis of how vorticity observed in the flow field contributes to the forces. Firstly we derive a potential flow model with vorticity concentrated in discrete vortices (Sec. 5.1). Then, we use this model to discuss the force generation mechanism (Sec. 5.2) and to clarify misconceptions on the bound vorticity (Sec. 5.3). Finally, the results and their significance are summarised in Sec. 6.

4 Impulse Theory

From Newton second law, we readily find that the force $\boldsymbol{F}$ on a body is given by the time derivative of the impulse. For a volume of fluid V_f with constant density ρ and velocity $\boldsymbol{u}$, whose external boundaries approach infinity,

$$\boldsymbol{F} = -\int_{V_f} \rho \frac{\mathrm{d}\boldsymbol{u}}{\mathrm{d}t}\,\mathrm{d}V = -\rho\frac{\mathrm{d}}{\mathrm{d}t}\int_{V_f} \boldsymbol{u}\,\mathrm{d}V = -\rho\frac{\mathrm{d}\boldsymbol{I}}{\mathrm{d}t}, \qquad (1)$$

where

$$\boldsymbol{I} = \int_{V_f} \boldsymbol{u}\,\mathrm{d}V \qquad (2)$$

is the impulse. Additional terms should be considered on the right hand side of eq. 2 to limit the boundary of the integral to an arbitrary finite volume [76–79], but this is not necessary for the scope of this work.

Burgers [80], Wu [81] and Lighthill [82] independently showed that the impulse is given by the sum of the integral over the fluid volume V_f of the first moment of the vorticity $\boldsymbol{\omega}$, and the integral over the solid surface S_b with outward unit normal $\boldsymbol{n}$ of the moment of tangential velocity:

$$\boldsymbol{I} = \frac{1}{n_d - 1}\left(\int_{V_f} \boldsymbol{x}\times\boldsymbol{\omega}\,\mathrm{d}V + \int_{S_b} \boldsymbol{x}\times(\boldsymbol{n}\times\boldsymbol{u})\,\mathrm{d}S\right), \qquad (3)$$

where $n_d = 2$ and 3 in two and three dimensions, respectively, and $\boldsymbol{x} = (x, y, z)$ is the coordinate vector. A complete derivation and discussion is available in, for instance, Eldredge [83] (p. 190).

The second term of eq. 3 vanishes in a reference system fixed with the body. This, in fact, is an unsteady body force equal to the difference between the forces as observed from the reference system $O(x, y, z)$ and those observed from a reference system fixed with the body. Furthermore, because it is proportional to the mass of the body [84, 85], it is negligible for small body to fluid density ratio [86] and for slender bodies with small volume to surface area ratio [87] such as sails. Therefore, for sail aerodynamics, the second term of eq. 3 is negligible for both rigid and flexible sails, independently of the reference system, while it should be considered to investigate, for example, the dynamics of flexible masts, which have a non-negligible volume.

This formulation (eq. 3), which Wu [81] and Lighthill [82] defined as the momentum theorem (based on vorticity moments) and impulse theory, respectively, allows computing the forces on a body from knowledge of the vorticity in the flow field. The convergence of the integral is not trivial because the vorticity might decay like x^{-2} and x^{-3} in two and three dimensions, respectively, and thus it just balances the rate at which the volume of the integral increases with the distance from the body [83] (p. 187). This is an issue that has to be carefully considered if the integral has to be numerically solved for steady conditions [88]. However, for one way around it is to consider a body starting from rest and a volume that includes the whole path travelled by the body, such that the vorticity is identically zero at the boundaries.

Key physical constrains that these models should satisfy are the Kutta condition and the Kelvin's theorem. In steady flow, the Kutta condition states that the flow velocity at the trailing edge of a slender body must be tangent to the bisector, or the trailing edge must be a stagnation point. In unsteady flow, it states that the flow must be tangent to one of the two sides of the trailing edge [71, 89]. For an infinitely thin plate, the plate-normal flow velocity at the trailing edge must vanish. In turn, this condition sets the amount of vorticity that is shed at the trailing edge by the solid body into the wake. The Kelvin's theorem states that, when the viscous dissipation of vorticity is negligible compared to its convection (e.g. at high Reynolds numbers) and zero net viscous torque is applied to the system by the body (e.g. for a non rotating sail), the integral of vorticity over the volume of fluid must vanish.

4.1 Bidimensional Flow

Let's consider a bidimensional space and a reference system fixed on the body that allows to simplify the derivation without loss of generality. The impulse formulation in eq. 1 and 3 becomes

$$\boldsymbol{F} = -\rho \frac{\mathrm{d}}{\mathrm{d}t} \int_{S_b} \boldsymbol{x} \times \boldsymbol{\omega_z} \, \mathrm{d}S. \tag{4}$$

Also consider the vorticity as concentrated in pairs of counter-rotating vortices with circulation $-\boldsymbol{\Gamma}$ and $\boldsymbol{\Gamma}$. We find that the force $\boldsymbol{F}$ in the direction orthogonal to the segment $\boldsymbol{d}$ from the centroid of the the vortex with negative circulation to that of positive circulation is [72, 90]:

$$\boldsymbol{F} = \rho \Sigma_i (\dot{\boldsymbol{\Gamma}}_i \times \boldsymbol{d}_i + \boldsymbol{\Gamma}_i \times \dot{\boldsymbol{d}}_i). \tag{5}$$

This is, in fact, the time derivative of the impulse of vortex pairs, whose impulse was found by Lamb [91] to be $\rho \Gamma d$. For a single vortex pair whose centroids of the two vortices are located at coordinate (x_1, y_1) and (x_2, y_2), eq. 5 shows that the lift (L) and drag (D) are

$$L = \rho \left((x_2 - x_1)\dot{\Gamma}_2 + (\dot{x_2} - \dot{x_1})\Gamma_2 \right), \tag{6}$$

$$D = -\rho \left((y_2 - y_1)\dot{\Gamma}_2 + (\dot{y_2} - \dot{y_1})\Gamma_2 \right). \tag{7}$$

This formulation is independent of the reference system. In the rest of the paper we consider a reference system with the x axis along the free stream velocity U and positive anticlockwise angles (Fig. 1).

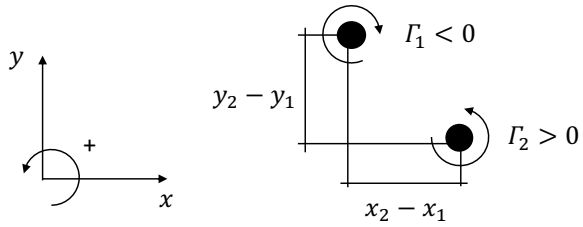

Figure 1: Coordinate system and vortex pair.

4.1.1 2D Plate at Low Incidence

Consider a flat plate with chord c at a small angle of attack α, starting from rest and reaching a steady velocity U (Fig. 2). The circulation is concentrated near the foil and in the region where the foil was at rest, while the net circulation in the wake must vanish in steady conditions. The wake is made of vortex pairs continuously generated on the two sides of the plates. The distance across which the vorticity is generated is roughly the plate thickness, which is small for a thin plate, thus $\boldsymbol{d} = (x_2 - x_1, y_2 - y_1) \approx (0, 0)$. Also, $\boldsymbol{d}$ remains of almost constant whilst the vortex pairs convect along the plate and then are shed into the wake, thus $\dot{\boldsymbol{d}} \approx (0, 0)$. Consequently, these vortex pairs do not contribute to lift nor drag. However, in the boundary layer there is a non zero net circulation. The integral of vorticity Γ_b around the plate is the bound circulation, while the integral of vorticity around the region where the plate was at rest is the starting circulation $-\Gamma_b$. The bound and starting vortex have constant circulation ($\dot{\Gamma}_b = 0$) and their distance increases at a rate $\dot{\boldsymbol{d}} = (U, 0)$.

The bound circulation can be computed by imposing the Kutta condition. For instance, by placing the bound vortex in the centre of the plate[1] and ensuring that its induced velocity at

[1] The bound vortex can be placed in the centre of the plate because the circulatory vortex sheet is symmetric around the centre of the plate

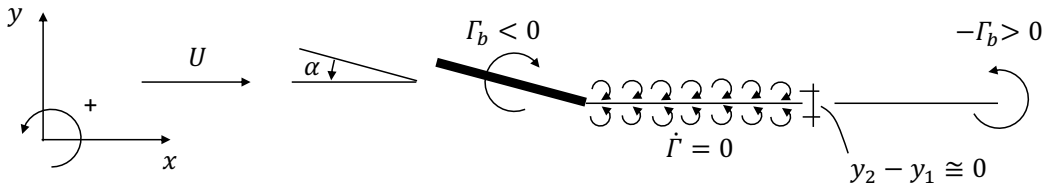

Figure 2: 2D plate at low incidence.

the trailing edge cancels the plate normal component of the free stream velocity, we find a negative bound circulation

$$\Gamma_b \approx -\pi U c \sin\alpha. \tag{8}$$

Inserting these values in eq. 6 and 7 gives the Kutta-Joukowski lift theorem and the d'Alembert's paradox, respectively:

$$L = -\rho U \Gamma_b = \rho U^2 c\,\pi \sin\alpha, \tag{9}$$

$$D \approx 0, \tag{10}$$

and in nondimensional form

$$C_L \approx 2\pi \sin\alpha, \tag{11}$$

$$C_D \approx 0. \tag{12}$$

These results are consistent with thin airfoil theory and in excellent agreement with experiments for $\alpha \lesssim 10°$. This interpretation of the Kutta-Joukowski lift theorem (eq. 9) reveals that the bound circulation is circulation that moves with velocity U, irrespectively of its nearness to the plate. In other words, all the vorticity in the flow field that moves with velocity U contributes to the bound circulation. This is also in agreement with the concept of trapped vortex studies by Saffman and Sheffield [92] and successively Huang and Chow [93]. A practical consequence of this result is that the lift can be estimated with eq. 9 by taking as bound circulation the integral of all of the vorticity in a time averaged flow field. This approach was adopted, for instance, by DeVoria and Mohseni [68], who considered various aspect ratio plates at various incidences. Because in steady conditions the net vorticity flux into the wake must vanish, the integral can be taken over a finite volume around the plate. For example, Lee et al. [67] investigated flat plates with aspect ratio between 1 and 3, at both low and high angles of attack, which are conditions relevant to yacht sails. They found that the forces computed by integrating the vorticity in the flow field do not vary when the integral is performed over a domain that extends beyond two or three chord lengths downstream of the plate.

4.1.2 2D Plate at High Incidence

Consider a flat plate at an angle of attack of approximately $\pi/2$ (Fig. 3). This flow condition was initially investigated as a potential flow with concentrated vorticity by von Helmholtz [94], who developed the free-streamline theory, and then further developed by von Kirchhoff [95] and Lord Rayleigh [96]. Vorticity is shed downstream through two shear layers of opposite sign and equal magnitude at the two edges of the plate. Most of this vorticity is generated at the edges. The vortex pair with size $\boldsymbol{d} = (c\cos\alpha, -c\sin\alpha)$, is shed rigidly downstream and thus $\dot{\boldsymbol{d}} = \boldsymbol{0}$.

An estimate of the production of vorticity can be derived from the integral of the flux of vorticity across the shear layers [97]. Consider a reference system $O'(x', y')$ with x' aligned with a shear layer of thickness δ_{SL}, with streamwise velocity u' ranging from 0 to U_{SL} (Fig. 3). The vorticity production is

$$|\dot{\Gamma}| = -\int_0^{\delta_{\mathrm{SL}}} \omega u' \,\mathrm{d}y' = \int_0^{\delta_{\mathrm{SL}}} \frac{\partial u'}{\partial y'} u' \,\mathrm{d}y' \tag{13}$$

$$= \int_0^{U_{\mathrm{SL}}} u' \,\mathrm{d}u' = \frac{1}{2} U_{\mathrm{SL}}^2. \tag{14}$$

A similar result was found accurate also in unsteady flow conditions [56, 89] for small angles of attack. Roshko [53] noted that at $\alpha = \pi/2$ and steady conditions, $U_{SL} = kU$ with k between 1.3 and 1.4. The interesting conclusion is that, if leading edge separation occurs and thus the Kutta condition is established at the leading edge, then there is a force contribution due to the vorticity production where $|\dot{\boldsymbol{\Gamma}}| = \dot{\Gamma} \approx k^2 U^2/2$. When substituted in eq. 6 and 7, we find that the force due to the production of vorticity is

$$L_p = \rho \dot{\Gamma} c \cos\alpha \approx \frac{1}{2}\rho U^2 c\, k^2 \cos\alpha, \tag{15}$$

$$D_p = \rho \dot{\Gamma} c \sin\alpha \approx \frac{1}{2}\rho U^2 c\, k^2 \sin\alpha. \tag{16}$$

Roshko [53] also notes that the distance between the two vortices of the vortex pair grows from c to $(1 + k')c$, with $k' \approx 0.35$. Let dt be the period of time over which this expansion occurs. The strength of the expanding vortex pair is the amount of vorticity produced over the period δt (i.e. $\dot{\Gamma}\delta t$), and the growth rate of the diameter of the vortex pair is $k'c/\delta t$, Hence, the vortex force contribution due to the wake size increasing is

$$L_v = \rho \dot{\Gamma} c\, k' \cos\alpha \approx \frac{1}{2}\rho U^2 c\, k' k^2 \cos\alpha, \tag{17}$$

$$D_v = \rho \dot{\Gamma} c\, k' \sin\alpha \approx \frac{1}{2}\rho U^2 c\, k' k^2 \sin\alpha. \tag{18}$$

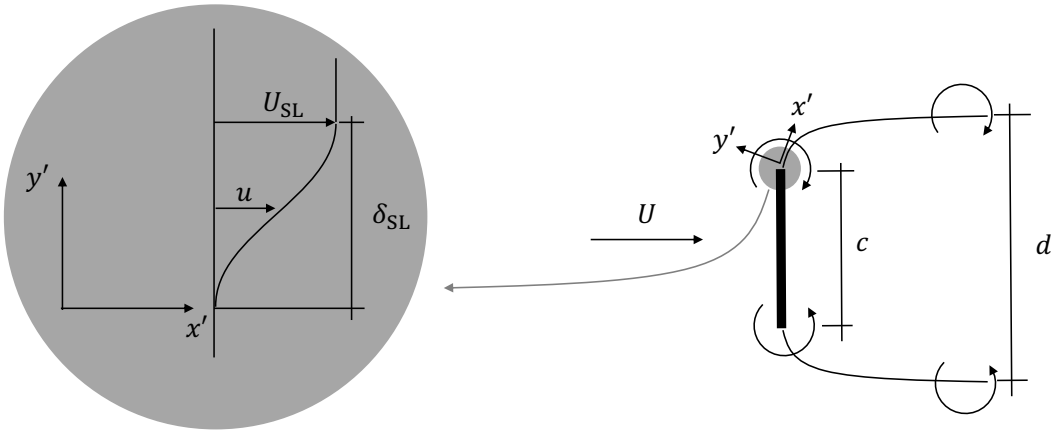

Figure 3: 2D plate at high incidence.

Hence, the lift and drag of a plate at high incidence is given by both the production of vorticity and the vortex dynamics. The sum of these contributions, in nondimensional form, is

$$C_L \approx (1 + k')k^2 \cos\alpha, \tag{19}$$

$$C_D \approx (1 + k')k^2 \sin\alpha. \tag{20}$$

The coefficients k and k' depend on the Reynolds number and can be measured from the flow field. For example, using $k = 1.3$-1.4 and $k' = 0.35$, eq. 19 and 20 give force coefficients that are in good agreement with those measured on a flat plate for α between $50°$ and $90°$ at Reynolds numbers of the order of 10^4 - 10^5 (e.g. [98]).

4.1.3 2D plate at moderate incidence

At those angles of attack between the stall angle, where leading edge separation occurs, and where the high-incidence model becomes accurate, we do not have a readily available model. The vorticity production is the same as at high incidence. Hence, there is a lift and drag contribution as given by eq. 15 and 16, respectively. Because the flow is not symmetrical around the streamwise direction, there must be bound circulation. Moreover, the vorticity shed by the leading and trailing edge might not convect uniformly downstream, leading to vortex forces. While the contribution due to the bound vorticity and the shed vortices is not easily quantifiable, some instructive observations can be made on both of them.

Firstly, when leading edge separation occurs, the bound circulation is positive and it generates a negative lift force! In particular, two vortex sheets of equal and opposite sign are shed by the two edges of the plate. The bound circulation ensures that the Kutta condition applies at the two edges. The sum of the plate-normal velocity components due to the vortex sheets, the free stream velocity and the bound circulation, must vanish. Assuming that the vortex sheets are parallel to the free stream velocity, and that their induced velocity on the opposite side of the plate is negligible, the reader can readily find that $\Gamma_b = \Gamma_0 \cos\alpha > 0$, where Γ_0 is constant with α. Therefore, there is a force component due to the bound circulation that is

$$L_b = -\rho U \Gamma_b = -\rho U \Gamma_0 \cos\alpha < 0, \tag{21}$$

$$D_b = 0. \tag{22}$$

This counter intuitive result can easily be verified with simulations or experiments by integrating the layer of vorticity enclosing the plate.

Furthermore, at moderate incidence, Babinsky et al. [72] noted that the vorticity shed at the leading edge convects downstream at about $U/2$, while the vorticity shed at the trailing edge convects with velocity U (Fig. 4). This is also consistent with the time-averaged results of DeVoria and Mohseni [68] on moderate incidence plates, where the time-averaged leading edge vorticity observed in the field of view (see FoV in Fig. 4) near the plate was about twice of the trailing edge vorticity. The slower convection of leading edge vorticity than trailing edge vorticity can occur only for a finite period of time δt. In fact, all of the vorticity in the wake must convect at the same velocity. Let assume, for example, that leading edge vorticity convects at $U/2$ for a length $c\cos\alpha$ and thus $\delta t = 2(c/U)\cos\alpha$. The additional vortex force due to the slow convection of leading edge vorticity $\Gamma_{\mathrm{LEV}} = -\dot{\Gamma}\delta t = -2\dot{\Gamma}(c/U)\cos\alpha$ is:

$$L_{\mathrm{LEV}} = -\rho\Gamma_{\mathrm{LEV}}\frac{U}{2} = \rho\dot{\Gamma}c\cos\alpha \approx \frac{1}{2}\rho U^2 c\, k^2 \cos\alpha, \tag{23}$$

Similarly, the cross-flow relative velocity of the LEV with respect to the TEV could be non zero for a finite period of time, leading to a drag force component.

Overall, the forces on a flat plate at moderate incidence are the sum of the positive effect of vorticity production, the negative effect of bound vorticity, and vortex forces due to the different velocity of the vorticity shed at the leading and trailing edge in a region near the plate. It must be noted that the

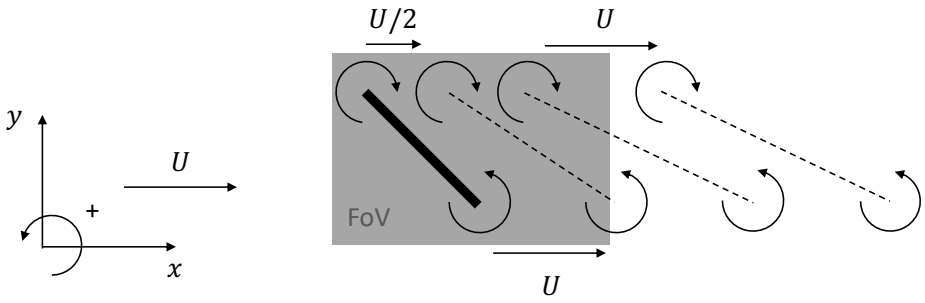

Figure 4: Vortex lift mechanism.

distinction between leading and trailing edge vorticity is unnecessary, and here used only to distinguish between negative and positive vorticity, respectively. In fact, to compute the forces with equation 5, the flow field must be described as an ensemble of vortex pairs with equal and opposite circulation. The choice of which positive vorticity is associated to which equal and opposite negative vorticity to form a vortex pair is arbitrary. Hence, this allows estimating the force due to the dynamics of any vorticity in the flow field.

4.2 Tridimensional Flow

In a tridimensional space, the akin of eq. 5 is

$$\boldsymbol{F} = \frac{1}{2}\rho\Sigma_i(\dot{\boldsymbol{\Gamma}}_i \times \boldsymbol{d}_i + \boldsymbol{\Gamma}_i \times \dot{\boldsymbol{d}}_i), \tag{24}$$

where the summation Σ is intended as a vectorial sum. The vorticity must be considered in all of the three planes. In other words, the total force on the body are the integral of the bidimensional forces in the three Cartesian planes! For example, consider planes orthogonal to the x axis and compute the force $\boldsymbol{F_{yz}}(x)$ based on the vorticity observed on that plane. Then integrate $\boldsymbol{F_{yz}}(x)$ along x. Repeat the same procedure for planes orthogonal to the y and the z axis to find the forces $\boldsymbol{F_{xz}}(y)$ and $\boldsymbol{F_{xy}}(z)$. The total force is

$$\boldsymbol{F} = \frac{1}{2}\left(\int \boldsymbol{F_{yz}}(x)\,\mathrm{d}x + \int \boldsymbol{F_{xz}}(y)\,\mathrm{d}y + \int \boldsymbol{F_{xy}}(z)\,\mathrm{d}z\right). \tag{25}$$

An example of how to implement this formula is provided in the following sections (Sec. 4.2.1 and 4.2.2). However, it is also useful to note that an alternative approach is to consider vortex rings. If we can consider the vorticity field as made of a combination of vortex rings, each with absolute strength Γ_j, minimum surface area spanned by the vortex loop A_j, and unit vector $\boldsymbol{n}_j$ normal to the surface and pointing in the opposite direction of the its axial induced velocity, then eq. 24 can be written as [99]

$$\boldsymbol{F} = \rho\Sigma_j(\dot{\Gamma}_j A_j + \Gamma_j \dot{A}_j)\,\boldsymbol{n}_j. \tag{26}$$

4.2.1 3D Plate at Low Incidence

Consider a plate with a chord c and span b at a small angle of attack α. The reference system $O(x, y, z)$ is placed at the leading edge at one end of the span, and has directions $\boldsymbol{i}, \boldsymbol{j}, \boldsymbol{k}$ in the drag, lift, and span direction respectively (Fig. 5). The plate forms a vortex ring enclosed between the plate's bound vortex, the two tip vortices and the starting vortex. Assuming the vortex ring as flat on the $y = 0$ plane, then the force is in the lift direction and eq. 25 becomes

$$\boldsymbol{F} = \boldsymbol{L} = \frac{1}{2}\left(\int_0^{c'} \boldsymbol{F_{yz}}(x)\,\mathrm{d}x + \int_0^{b} \boldsymbol{F_{xy}}(z)\,\mathrm{d}z\right), \tag{27}$$

where $c' = c\cos\alpha$. The strength of the vortex ring is constant and equal to the bound vorticity Γ_b. The ring size along the streamwise direction grows with velocity U, sustained by a production of vorticity $\dot{\Gamma}_b = \Gamma_b U/c'$ at the two tips. The two integrals in eq. 27 are identical and, hence, the tridimensional and bidimensional solutions give the same force per unit span (cf. eq. 9):

$$\boldsymbol{L} = -\frac{\rho}{2}\left((\Gamma_b U/c')bc' + U\Gamma_b b\right)\boldsymbol{j} = -\rho U\Gamma_b b\,\boldsymbol{j}, \tag{28}$$

$$\boldsymbol{C_L} = -2\frac{\Gamma_b}{Uc}\boldsymbol{j}. \tag{29}$$

The same results can be achieved using eq. 26 noting that $\dot{A} = Ub$.

In the above derivation we assumed the vortex ring to be approximately flat but, indeed, it is is at a small angle with the free stream. If fact ,due to its own induced velocity, the tip vortices convect along $\boldsymbol{j}$ with velocity V (with $|V| \ll |U|$), which is the downwash velocity. This results in a drag force akin to that for the lift:

$$\boldsymbol{D} = -\rho V\Gamma_b b\,\boldsymbol{i}, \tag{30}$$

$$\boldsymbol{C_D} = -2\frac{V}{U}\frac{\Gamma_b}{Uc}\boldsymbol{i}. \tag{31}$$

These lift and drag results (eq. 28 and 30) are consistent with lifting line theory [100] and were independently derived by Lanchester [4] and Prandtl [101]. They provide accurate results at small angles of incidence, where there is no leading edge separation.

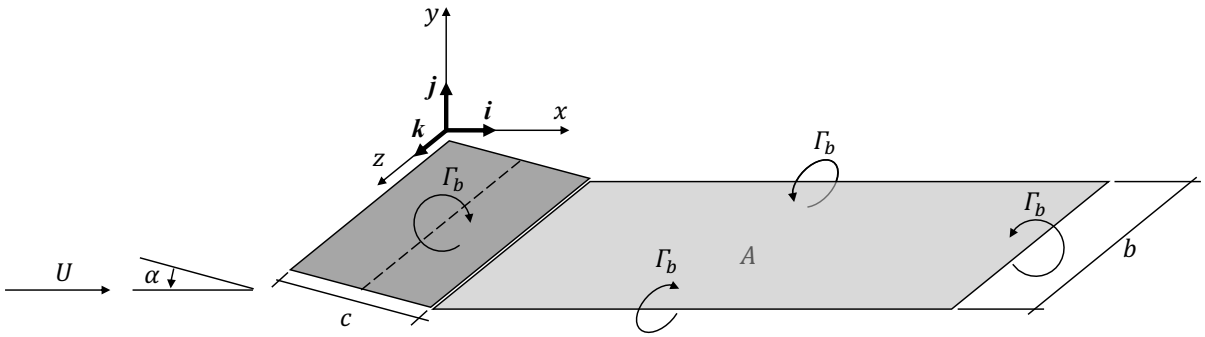

Figure 5: 3D plate at low incidence.

4.2.2 3D Plate at High Incidence

Consider a plate at high incidence. In this case, a vortex ring is continuously generated on the plane of the plate and shed downstream in the streamwise direction (Fig. 6). In this case, the direction orthogonal to the vortex ring is the plate-normal direction and eq. 25 becomes

$$\boldsymbol{F} = \boldsymbol{F_n} = \frac{1}{2}\left(\int_0^c \boldsymbol{F_{yz}}(x)\,\mathrm{d}x + \int_0^b \boldsymbol{F_{xy}}(z)\,\mathrm{d}z\right). \quad (32)$$

As for the bidimensional case, we can identify a force due to the vorticity production, which is constant and uniform along the perimeter of the plate, and a vortex force due to the growth of the wake diameter, i.e. of the vortex ring's enclosed area. For both of these force components, the integrals in eq. 32 are identical and, hence, the tridimensional and bidimensional formulations give the same force per unit span. For example, the force due to the production of vorticity, which is the dominant force generation mechanism for low aspect ratio plates, is (see eq. 16):

$$|\boldsymbol{F_n}| = \frac{\rho}{2}\left(\dot{\Gamma}bc + \dot{\Gamma}cb\right) = \rho\dot{\Gamma}bc. \quad (33)$$

The same results can be achieved using eq. 26 noting that $A = bc$. This force is made of the two components in the lift and drag directions

$$\boldsymbol{L} = \rho\dot{\Gamma}bc\cos\alpha\,\boldsymbol{j}, \quad (34)$$

$$\boldsymbol{D} = \rho\dot{\Gamma}bc\sin\alpha\,\boldsymbol{i}, \quad (35)$$

and in non dimensional form,

$$\boldsymbol{C_L} = 2\frac{\dot{\Gamma}}{U^2}\cos\alpha\,\boldsymbol{j}. \quad (36)$$

$$\boldsymbol{C_D} = 2\frac{\dot{\Gamma}}{U^2}\sin\alpha\,\boldsymbol{i}. \quad (37)$$

Assuming $\dot{\Gamma} = U^2/2$ as in eq. 13, this formulation without the vortex contribution gives $C_L = 0$ and $C_D = 1$ for $\alpha = \pi/2$. This is consistent with flat plate experiments [102], where C_D decreases from 2 for an infinite aspect ratio to 1.5, 1.2 and 1.18 for a plate with aspect ratio 20, 5 and 2, respectively (White [102] states that these results are valid for Reynolds numbers of at least 10^4).

5 Force Contribution of Free Vorticity in the Fluid

As highlighted in Sec. 3, a key advantage of the proposed approach is that it allows interpreting the contribution of any nucleus of vorticity to the force generation. In this section we consider the effect of free vorticity outside of the boundary layer on the forces, and also on the vorticity within the boundary layer (i.e. on the bound vorticity). To investigate, we consider a generic velocity and a vorticity field that could represent the result of a numerical simulation or of flow visualisation. In the following section (Sec. 5.1) we derive this flow field analytically. However, our aim is to provide guidelines on how measured or computed flow fields can be interpreted.

5.1 Complex Potential of an Example Flow Field

We approximate a sail section with a circular arc, and we compute the bound vorticity that is necessary to ensure the Kutta condition through a Kutta-Joukowski transformation [103]. Here we follow the approach of Arredondo-Galeana and Viola [18]. We consider a free stream velocity U and a doublet, such that it results in a cylinder of radius R. We add a vortex with circulation Γ_b at the centre of the cylinder (Fig. 7). The centre of the cylinder is placed in a complex coordinate reference system at $\zeta_0 = \mu i$, such that the transformed cylinder is a curved plate with maximum camber 2μ. We add a free vortex with circulation Γ_v equal to the integral of the region of vorticity outside of the cylinder, at the complex coordinate $\zeta_v = \rho_v e^{i\tau_v} + \mu e^{i\pi/2}$, where ρ_v and τ_v are the radial and azimuthal coordinate of the vortex, respectively. The vortex has a mirror vortex inside of the cylinder at $\zeta_v' = (R^2\rho_v^{-1})e^{i\tau_v} + \mu e^{i\pi/2}$ to maintain the non penetration condition on the cylinder. The sum of the bound circulation and of the image vortex circulation, $\Gamma_b - \Gamma_v$ (where $-\Gamma_v$ is

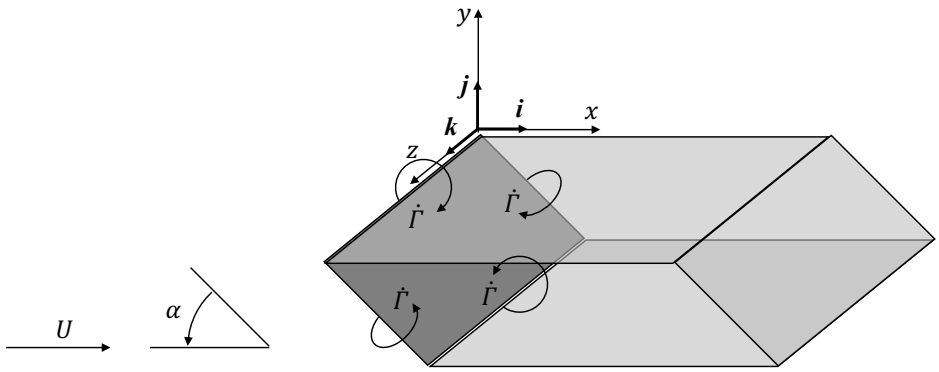

Figure 6: 3D plate at high incidence.

the image vortex circulation), is the vorticity in the boundary layer. Because we want Γ_b to represent the total vorticity within the boundary layer, we add an additional vortex Γ_v in the centre of the cylinder. Hence, the combined effect of $-\Gamma_v$ at the image vortex location and Γ_v in the centre of the vortex is simply to redistribute within the boundary layer the total amount of vorticity Γ_b. [2] While this model includes only one external vortex, any number of vortices can be included in the same manner.

The overall complex potential is

$$F(\zeta) = U(\zeta - \zeta_0)e^{-i\alpha} + \frac{UR^2 e^{i\alpha}}{(\zeta - \zeta_0)} \tag{38}$$

$$- \frac{i(\Gamma_\mathrm{b} + \Gamma_v)}{2\pi} \ln(\zeta - \zeta_0) - \frac{i\Gamma_v}{2\pi} \ln \frac{\zeta - \zeta_v}{\zeta - \zeta_v'}, \tag{39}$$

where α is the angle of incidence. The complex velocity in the cylinder plane is given by differentiating the complex potential with respect to ζ, that is

$$W(\zeta) = \frac{\mathrm{d}F(\zeta)}{\mathrm{d}\zeta} \tag{40}$$

$$= Ue^{-i\alpha} - \frac{UR^2 e^{i\alpha}}{(\zeta - \zeta_0)^2} - \frac{i(\Gamma_\mathrm{b} + \Gamma_v)}{2\pi} \frac{1}{\zeta - \zeta_0} \tag{41}$$

$$- \frac{i\Gamma_v}{2\pi} \left[\frac{1}{\zeta - \zeta_v} - \frac{1}{\zeta - \zeta_v'} \right]. \tag{42}$$

The real and imaginary part of the complex velocity give the streamwise and cross-flow velocity component, respectively. The resulting flow field can be mapped into the sail plane with the transformation

$$z = \left(\zeta + \frac{(R\cos\beta)^2}{\zeta} \right) e^{-i\alpha}. \tag{43}$$

[2] With the proposed approach, which is the same as in Pitt Ford and Babinsky [104], we consider the bound vortex and the external vortex as separate identities. For example, the external vortex could be a vortex gust. It should be noted that an alternative approach is to consider the external vortex as vorticity that was in the boundary layer such as, for example, in Corkery et al. [105]. In this latter case, we no longer add an additional vortex Γ_v in the centre of the cylinder, Γ_b is the vorticity that was originally in the boundary layer, while $\Gamma_b - \Gamma_v$ is the remaining vorticity in the boundary layer after Γ_v has been shed.

The bound circulation that ensures the Kutta condition is found by the additional condition that the sail trailing edge on the cylinder plane, $\zeta_\mathrm{TE} = R\,e^{-i\beta} + i\mu = 0$, is a stagnation point, i.e. $W(\zeta_\mathrm{TE}) = 0$.

Finally, solving eq. 40 for Γ_b we find an expression for the bound circulation as a function of the circulation and position of the external vortex: [18]

$$\Gamma_b = -4R\pi U \sin(\alpha + \beta) - \kappa\Gamma_v, \tag{44}$$

where $\beta = \mathrm{atan}(4\mu/c)$ is the effective angle of attack due to the sail curvature, and

$$\kappa = 2R \frac{R - \rho_v \cos(\beta + \tau_v)}{R^2 + \rho_v^2 - 2R\rho\cos(\beta + \tau_v)}. \tag{45}$$

The first term on the right hand side of eq. 44 is the bound circulation of a cylinder without an external vortex. Because it is negative, it generates a positive lift. The presence of the external vortex modifies the bound circulation by the coefficient κ, which depends on the spatial location of the vortex with respect to the sail. The effect of the extrenal vortex on the force generation is discussed in the next two sections (Sec. 5.2 and 5.3). The contours of κ in the cylinder and sail plane are shown in Fig. 8a and b, respectively. The figure also show an example of streamlines for the arbitrary position and strength of an external vortex.

5.2 Force Production Mechanism

For the flow condition described in Sec. 5.1, where leading edge separation does not occur, the generation of vorticity is negligible and thus we have not included any source of vorticity in our model. The whole vorticity in the region near the sail is modelled by two vortices: the external vortex and a vortex with circulation Γ_b representing the overall vorticity in the boundary layer (the position of this vortex within the sail depends on the position of the external vortex because of its image vortex). The force generation mechanisms is due to the dynamics of the existing vortex pairs, which can be arbitrary

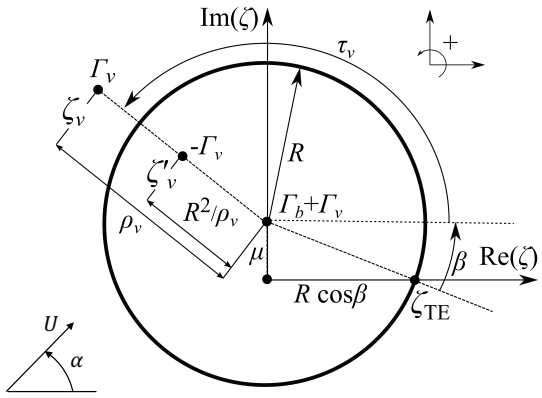

Figure 7: Complex plane of a rotating cylinder with an external vortex.

chosen as long as all the circulation is accounted for and that the net circulation is zero to satisfy Kelvin's theorem. If the net observable vorticity is not zero, then there must be circulation with equal magnitude and opposite sign somewhere far away along the wake. For example, let's consider the vortex pair made of Γ_b in the boundary layer and $-\Gamma_b$ at an infinite distance downstream of the sail, and the vortex pair made of Γ_v near the sail and $-\Gamma_v$ infinitely downstream. The force is due to the change in size and orientation of these two vortex pairs.

The bound circulation is moving away from the starting vortex at velocity U, thus leading to the Kutta-Joukowski lift (eq. 9): $L_b = -\rho U \Gamma_b$. The contribution of the free vortex is not as straight forward because its velocity depends on its position. If we use this approach to interpret the results of a numerical or experimental flow field, a critical distinction must be made. If the flow is instantaneous, the velocity of the circulation Γ_v could be approximated by the average velocity in the region occupied by the vorticity (better if the average is weighted by the distribution of vorticity). Its force contribution is zero only if the free vortex convects downstream with velocity U, which is equivalent to the convection of the vortex pair being frozen. For example, if this vortex was a vortex gust in turbulent flow and its trajectory was unchanged by the sail, it would have no force contribution. Conversely, if the free vortex is close enough to the sail such that the velocity induced by the bound circulation on the free vortex is not negligible, then the vortex pair would be modified giving rise to a gust force. Specifically, if the streamwise velocity of a vortex with positive circulation is higher than U, it generates a positive lift, and vice versa if the circulation is negative (e.g. the LEV in eq. 23). If the vertical velocity of a vortex with positive circulation is positive, it generates thrust, and it generates drag if the circulation is negative.

5.3 Effect of a Free Vortex on the Bound Vortex

The effect of the free vortex on the bound circulation can be deducted from equations 44 and 45. In deriving this equation we have assumed that the bound circulation is such that it ensures the Kutta condition. The addition of free vorticity in the surrounding fluid contributes with an induced velocity at the trailing edge, thus resulting in different value of the bound circulation. If the free vortex is on the sail surface, then $\kappa = 1$ and the bound circulation is reduced precisely by the free vortex circulation (Fig. 8). Its effect decreases with the distance from the sail.

Let's consider, for example, a realistic flow field with leading edge separation and time averaged reattachment. The vorticity in the LEV contributes to the generation of induced velocity at the trailing edge and thus the bound circulation must be lower than it would have been without LEV. Therefore, while the LEV provides a positive lift contribution (see eq. 23), it also leads to a lower bound circulation. The sum of the two effects cancel each other perfectly if the LEV remains in a fixed position with respect to the sail (see Saffman and Sheffield's [92] trapped vortex) and at this position $\kappa \approx 1$. The lift enhancing mechanism of the LEV, firstly observed by Ellington [106] and then well documented by many others [107–115], must be referred to the difference in lift between a wing with LEV and a wing otherwise stalled. In fact, the main role of the LEV is to retain leading edge vorticity near the sail instead of letting it convect downstream at the freestream velocity.

5.4 Time-Averaged Forces

If the flow field is time averaged, the velocity of any observed vorticity is null. In fact, that is the vorticity that, on average, is found at that location. Hence, we cannot use equation eq. 5 or 24 because we cannot observe $\dot{\boldsymbol{d}}$. However, the time-averaged vorticity observed near the plate is, on average, moving with the wing. Therefore, we found that the Kutta-Joukowski lift formula holds also for a time-averaged flow field where the bound circulation is the integral of all of the observed time-averaged vorticity within a region including the sail and intersecting the wake orthogonally. The lift contribution of the vorticity production and of the vortex lift contribution of repeatedly shed vortices is not neglected but implicitly included. In fact, the lower the flow velocity convecting vorticity through an arbitrary volume, the higher the time averaged value of vorticity in the volume.

The time-averaged drag can be estimated using Taylor's formula (Taylor's Appendix in Bryan et al. [116]),

$$D = \int_W (p - p_0) \mathrm{d}y, \tag{46}$$

which states that the drag is the integral over a line W intersecting orthogonally the wake, of the difference between the

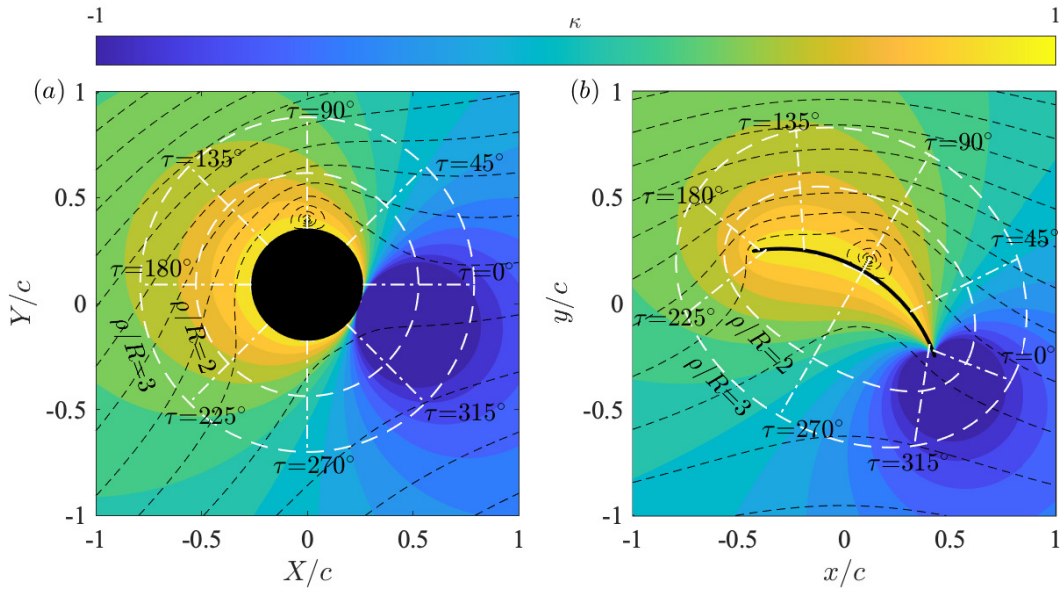

Figure 8: Contour of κ on the cylinder plane ζ (a) and the sail plane z. White dotted lines show the radial and azimuthal coordinates ρ and τ. Black lines show an example of streamlines for the arbitrary set of values $\Gamma_b/(cU) = 0.26$, $\Gamma_v/(cU) = 2.5$, $\rho/R = 1.15$ and $\tau = \pi/2$.

pressure in the wake p and that in the far field p_0. By using the Bernoulli equation, this equation shows that the drag is equal to the momentum loss in the wake, a result directly verifiable by applying Newton's second law. Wu et al. [99] recently showed that the first order approximation of eq. 46 is

$$D = -\rho U \int_W yw\mathrm{d}y, \tag{47}$$

thus enabling the use of Taylor's formula by knowledge of only the vorticity field along W. For example, a bidimensional plate with chord c at incidence α that generates vorticity at a rate $\dot{\Gamma}$, forms two shear layers with strength $\gamma = \dot{\Gamma}/U$ that extend from each edge of the plate to infinity. The shear layers are the only vorticity that intersects W and thus eq. 47 becomes

$$D = \rho U \gamma c \sin\alpha = \rho \dot{\Gamma} c \sin\alpha. \tag{48}$$

Substituting $\gamma = \dot{\Gamma}/U$ in eq. 48, we find precisesly eq. 16.

Liu et al. [9] showed that eq. 47 is equivalent to Filon's drag formula when the shear layer approximation $\partial/\partial y \gg \partial/\partial x$ is used. Therefore, eq. 47 is a form of the Filon's formula that, together with the Kutta-Joukowski formlulation, allows the computation of the time-averaged lift and drag. These two equations together, that we call the Kutta-Joukowski-Filon equations, can be combined into one vectorial equation and extended to tridimensional flow as [117]

$$\boldsymbol{F} = \rho \boldsymbol{U} \times \boldsymbol{\Gamma_b} + \rho \boldsymbol{U} Q, \tag{49}$$

where

$$Q = \frac{1}{n_d - 1} \int_{S_W} (z\omega_y - y\omega_z)\mathrm{d}S, \tag{50}$$

$n_d = 2$ and 3 in two and three dimensions, respectively. S_W is a plane orthogonally intersecting the wake. For example, for a plate with span b and chord c at incidence α, eq. 49 becomes

$$\boldsymbol{F} = \rho U \Gamma_b b\, \boldsymbol{j} + \rho U \gamma b c \sin\alpha\, \boldsymbol{i}. \tag{51}$$

Noting that $\gamma = \dot{\Gamma}/U$, this result is consistent with eq. 28 and 35.

6 Discussion and Conclusions

Sail aerodynamics have been traditionally explained through thin airfoil theory and lifting line theory. However, the underlying assumptions of these theories are not compatible with separated flow, which is an inherent feature of yacht sails. Therefore, a new paradigm is proposed, that is compatible with both attached and separated flow conditions. Based on the impulse theory, this paradigm enables an intuitive and in-depth understanding of some of the key results of thin airfoil theory and lifting line theory. In addition, it provides an intuitive interpretation of the force contribution of any vorticity in the flow field. Hence, the proposed approach can guide sail designers to improve sail performances also when flow separation prevent them from using potential flow theories.

The proposed paradigm is as follows. To ensures the non-slip and non-penetration condition, the sail must generate vorticity. The vorticity in the fluid is exactly what is needed to ensure these two conditions. The Kutta condition and Kelvin's theorem set two further conditions that make this vorticity field completely determined, both in the boundary layer and

infinitely far from the sail. This vorticity field can be described as an ensemble of vortex rings (which degenerate in vortex pairs in two dimensions). The forces on the sail are the rate of change of the impulse $\boldsymbol{I}$ of the vortex rings:

$$\boldsymbol{F} = \rho \frac{\mathrm{d}\boldsymbol{I}}{\mathrm{d}t} = \rho \Sigma_j (\dot{\Gamma}_j A_j + \Gamma_j \dot{A}_j)\, \boldsymbol{n}_j. \tag{52}$$

There are three key force generation mechanisms associated with three different ways of changing the impulse: (1) varying the circulation Γ_j; (2) varying the area of the enclosed surface A_j; (3) rotating the vortex ring and thus the orientation of $\boldsymbol{n}_j$. The force experienced by a sail is the sum of the force contributions of these three mechanisms.

1. The first one is that employed by parachutes, whose continuous generation of vortex rings parallel to the parachute surface results in a drag that is $D = \rho \dot{\Gamma} A$. For a yacht sail, whose surface is not perpendicular to the wind as the parachute, this force contribution has both a lift and a drag component.
2. The second mechanism, is that employed by an airplane wing at low incidence. The vortex ring is enclosed between the wing of span b, the tip vortices and the starting vortex. The area of the vortex ring increases at a rate $\dot{A} = Ub$, resulting in a lift $L = \rho U b \Gamma$.
3. The parachute-type vortex ring generated around the sail surface might change shape and orientation in the first few convective lengths before being shed into the wake, resulting in an additional vortex force of the type $F = \rho\, (\delta U)\, b\Gamma$, where δU is the difference in velocity between different legs of the vortex ring. Any element of vorticity around the sail is part of a vortex ring and its force contribution is associated with the change of its area and orientation before it is shed into the wake.

Based on this paradigm, we showed that the knowledge of the instantaneous vorticity and velocity field allows the computation/interpretation of the instantaneous lift and drag. Moreover, we also showed that the time-averaged vorticity field alone is sufficient to compute/interpret the time-averaged lift and drag by using the Kutta-Joukowski-Filon equation.

Acknowledgements

This paper is dedicated to Arvel Gentry, whose dedication to public outreach inspired generations of sail aerodynamicists.

REFERENCES

[1] Ed Regis. The Enigma of Aerodynamic Lift. *Sci. Am.*, 322(2):44–51, 2020.

[2] Arvel Gentry. How Sails Really Work. *Sail Mag.*, (April), 1973.

[3] A Gentry. What goes around comes around. *Sail. World*, 1991.

[4] Frederick William Lanchester. *Aerodynamics: constituting the first volume of a complete work on aerial flight*, volume 1. London, A. Constable & Co., Ltd., 1907.

[5] W M Kutta. Auftreibskrafte in Stromenden Flussigkeiten. *lilust. Aeronaut. Mitt.*, 1902.

[6] N E Jowkowski. On annexed vortices. *Proc. Phys. Sect. Nat. Sci. Soc.*, 13(2):12–25, 1906.

[7] J H Milgram. Sailing vessels and sails. *Annu. Rev. Fluid Mech.*, 4(397-430), 1972.

[8] L N G Filon. The forces on a cylinder in a stream of viscous fluid. *Proc. R. Soc. London. Ser. A, Contain. Pap. a Math. Phys. Character*, 113(763):7–27, 1926.

[9] L. Q. Liu, J. Y. Zhu, and J. Z. Wu. Lift and drag in two-dimensional steady viscous and compressible flow. *J. Fluid Mech.*, 784:304–341, 2015.

[10] Tom Whidden and Michael Levitt. *The Art and Science of Sails: A Guide to Modern Materials, Construction, Aerodynamics, Upkeep, and Use*. First edition, 1990.

[11] Lars Larsson and Rolf E Eliasson. *Principles of yacht design*. Society of Naval Architects & Marine Engineers, first amer edition, 1995.

[12] A. R. Claughton, R. A. Shenoi, and J. F. Wellicome. *Sailing Yacht Design: Theory*. First edition, 1998.

[13] Fabio Fossati. *Aerodynamics and the performance of sailing yacht*. 2009.

[14] Peter van Oossanen. *The Science of Sailing: Part 2*. Van Oossanen Academy, first edit edition.

[15] Arvel Gentry. The Aerodynamics of Sail Interaction. *Third AIAA Symp. AeroHydrodnautics Sail.*, pages 1–12, 1971.

[16] By Arvel Gentry. More on the Slot Effect. (August):2–4, 1973.

[17] Ignazio Maria Viola, Simone Bartesaghi, Thomas Van-Renterghem, and Raffaele Ponzini. Detached Eddy Simulation of a Sailing Yacht. *Ocean Eng.*, 90:93–103, 2014.

[18] Abel Arredondo-Galeana and Ignazio Maria Viola. The leading edge vortex of yacht sails. *Ocean Eng. Virtual Spec. Issue Yacht Eng. 2017*, page 11, 2018.

[19] P.R. Owen and L. Klanfer. On the Laminar Boundary Layer Separation from the Leading edge of a Thin Aerofoil. Technical Report 220, 1955.

[20] Donald E. Gault. An investigation at low speed of the flow over a simulated flat plate at small angles of attack using pitot-static and hot-wire probes. *Natl. Advis. Comm. Aeronaut.*, 1957.

[21] P K Chang. Leading-edge Flow Separation. In *Sep. Flow*, pages 452–530. 1970.

[22] A. V. Arena and T. J. Mueller. Laminar separation, transition, and turbulent reattachment near the leading edge of airfoils. *AIAA J.*, 18(7):747–753, 1980.

[23] J E Carter and V N Vatsa. Analysis of Airfoil Leading Edge Separation. Technical report, 1984.

[24] JW Newman and MC Tse. Incompressible flow past a flat plate aerofoil with leading edge separation bubble. *Aeronaut. J.*, 96:57–64, 1992.

[25] M J Crompton and R V Barrett. Investigation of the separation bubble formed behind the sharp leading edge of a flat plate at incidence. *Proc. Inst. Mech. Eng. Part G J. Aerosp. Eng.*, 214:157–176, 2000.

[26] J P J Stevenson, K P Nolan, and E J Walsh. Particle image velocimetry measurements of induced separation at the leading edge of a plate. *J. Fluid Mech.*, 804:278–297, 2016.

[27] J P J Stevenson, E J Walsh, and K P Nolan. Visualization of the vortex and reverse-flow structure of a separation bubble. *J. Vis.*, 19:175–177, 2016.

[28] Ignazio Maria Viola and Richard G J Flay. Sail aerodynamics: understanding pressure distributions on upwind sails. *Exp. Therm. Fluid Sci.*, 35(8):1497–1504, 2011.

[29] Ignazio Maria Viola, J P Pilate, and R G J Flay. Upwind sail aerodynamics: A pressure distribution database for the validation of numerical codes. *Int. J. Small Cr. Technol.*, 153(1):47–58, 2011.

[30] I M Viola, P Bot, and M Riotte. Upwind sail aerodynamics: A RANS numerical investigation validated with wind tunnel pressure measurements. *Int. J. Heat Fluid Flow*, 39:90–101, 2013.

[31] I. M. Viola and R. G. J. Flay. Aerodynamics of headsails: a review of measured surface pressures and expected flow fields. In *5th High Perform. Yacht Des. Conf.*, Auckland, New Zealand, 2015.

[32] J-B R G Souppez, A Arredondo-Galeana, and I M Viola. Recent Advances in Downwind Sail Aerodynamics. *23rd Cheasapeake Sail. Yacht Symp.*, (March), 2019.

[33] Jean-Baptiste R G Souppez, Abel Arredondo-Galeana, and Ignazio Maria Viola. Recent Advances in Numerical and Experimental Downwind Sail Aerodynamics. *J. Sail. Technol.*, 4(01):45–65, 2019.

[34] Ignazio Maria Viola, S Bartesaghi, T Van Renterghem, and R Ponzini. Delayed detached eddy simulation of sailing yacht sails. In *3rd Int. Conf. Innov. High Perform. Sail. Yachts*, 2013.

[35] T. Maxworthy. The formation and maintenance of a leading-edge vortex during the forward motion of an animal wing. *J. Fluid Mech.*, 587:471–475, 2007.

[36] A. Widmann and C. Tropea. Parameters influencing vortex growth and detachment on unsteady aerodynamic profiles. *J. Fluid Mech.*, 773:432–459, 2015.

[37] James M. Akkala and James H.J. Buchholz. Vorticity transport mechanisms governing the development of leading-edge vortices. *J. Fluid Mech.*, 829:512–537, 2017.

[38] Mathew F. Marzanek and David E. Rival. Separation mechanics of non-slender delta wings during streamwise gusts. *J. Fluids Struct.*, 90:286–296, 2019.

[39] Jeff D Eldredge and Anya R Jones. Leading-Edge Vortices: Mechanics and Modeling. *Annu. Rev. Fluid Mech.*, 51(August 2018):75–104, 2019.

[40] J Deparday, P Bot, F Hauville, B Augier, M Rabaud, D Motta, and D Le Pelley. Modal analysis of pressures on a full-scale spinnaker. In *22nd Chesap. Sail. Yacht Symp.*, pages 98–110, Annapolis, MD, 2016. SNAME.

[41] J H Milgram. Fluid mechanics for sailing vessel design. *Annu. Rev. Fluid Mech.*, 30(Milgram 1996):613–653, 1998.

[42] Ignazio Maria Viola. Recent advances in sailing yacht aerodynamics. *Appl. Mech. Rev.*, 65(4):1–12, 2013.

[43] V Cisotti. Moto con scia di un profilo flessibile, Nota I and II. *Rend, della R. Accad. Naz. dei Lincei*, 15, 1932.

[44] Kurt Voelz. Profil und auftrieb eines segels. *ZAMMJournal Appl. Math. Mech. für Angew. Math. und Mech.*, 30(10):301–317, 1950.

[45] B Thwaites. The aerodynamic theory of sails. I. Two-dimensional sails. *Proc. R. Soc. London. Ser. A. Math. Phys. Sci.*, 261(1306):402–422, 1961.

[46] J. P. Dugan and Since Cisotti. A free-streamline model of the two-dimensional sail. *J. Fluid Mech.*, 42(3):433–446, 1970.

[47] Rick Smith and Wei Shyy. Computation of unsteady laminar flow over a flexible twodimensional membrane wing. *Phys. Fluids*, 7(9):2175–2184, 1995.

[48] Jack N Nielsen. Theory of flexible aerodynamic surfaces. 1963.

[49] Richard Smith and Wei Shyy. Computational model of flexible membrane wings in steady laminar flow. *AIAA J.*, 33(10):1769–1777, 1995.

[50] Rick Smith and Wei Shyy. Computation of aerodynamic coefficients for a flexible membrane airfoil in turbulent flow: A comparison with classical theory. *Phys. Fluids*, 8(12):3346–3353, 1996.

[51] Arnold Song, Xiaodong Tian, Emily Israeli, Ricardo Galvao, Kristin Bishop, Sharon Swartz, and Kenneth Breuer. Aeromechanics of membrane wings with implications for animal flight. *AIAA J.*, 46(8):2096–2106, 2008.

[52] Rye M Waldman and Kenneth S Breuer. Camber and aerodynamic performance of compliant membrane wings. *J. Fluids Struct.*, 68:390–402, 2017.

[53] Anatol Roshko. On the drag and shedding frequency of two dimensional bluff bodies. *NACA TN 3169*, 1954.

[54] Anatol Roshko. On the Wake and Drag of Bluff Bodies. *J. Aeronaut. Sci.*, 22(2):124–132, 1955.

[55] Turgut Sarpkaya. An inviscid model of two-dimensional vortex shedding for transient and asymptotically steady separated flow over an inclined plate. *J. Fluid Mech.*, 68(1):109–128, 1975.

[56] M Kiya and M Arie. an Inclined Flat Plate in Uniform Flow. *J. Fluid Mech.*, 82(1977), 1977.

[57] Imran Afgan, Sofiane Benhamadouche, Xingsi Han, Pierre Sagaut, and Dominique Laurence. Flow over a flat plate with uniform inlet and incident coherent gusts. *J. Fluid Mech.*, 720:457–485, 2013.

[58] Shigeru Sunada, Akitoshi Sakaguchi, and Keiji Kawachi. Airfoil Section Characteristics at a Low Reynolds Number. *J. Fluids Eng.*, 119(1):129, 1997.

[59] S. Sunada, T. Yasuda, K. Yasuda, and K. Kawachi. Comparison of wing characteristics at an ultralow Reynolds number. *J. Aircr.*, 39(2):331–338, 2002.

[60] M Okamoto and Akira Azuma. Experimental Study on Aerodynamic Characteristics of Unsteady Wings at Low Reynolds Number. *AIAA J.*, 43(12):3–6, 2005.

[61] S Nava, P Bot, J Cater, and S E Norris. Modelling the Lift Crisis of a Cambered Plate at 0 deg Angle of Attack. In *20th Australas. Fluid Mech. Conf.*, number December, pages 6–9, Perth, 2016.

[62] S J Collie, P S Jackson, J B Fallow, and M Gerritsen. Two-Dimensional CFD-Based Parametric Analysis of Downwind Sail Designs. *Int. J. Small Cr. Technol.*, 146(b1):15, 2004.

[63] Stéphane Cyr and Jacques Estelle. *A theoretical Model for Flow about a circular-arc Aerofoil with Separation Thesis by*. PhD thesis, McGill University, 1992.

[64] Patrick Bot, Marc Rabaud, Goulven Thomas, Alessandro Lombardi, and Charles Lebret. Sharp Transition in the Lift Force of a Fluid Flowing Past Nonsymmetrical Obstacles: Evidence for a Lift Crisis in the Drag Crisis Regime. *Phys. Rev. Lett.*, 117(23):234501, 2016.

[65] P Bot. Force Variations Related to Flow Pattern Changes Around a High-Camber Thin Wing. *AIAA J.*, pages 1–7, 2019.

[66] Kunihiko Taira and Tim Colonius. Three-dimensional flows around low-aspect-ratio flat-plate wings at low Reynolds numbers. *J. Fluid Mech.*, 623:187–207, 2009.

[67] Jian Jhih Lee, Cheng Ta Hsieh, Chien C. Chang, and Chin Chou Chu. Vorticity forces on an impulsively started finite plate. *J. Fluid Mech.*, 694:464–492, 2012.

[68] Adam C. Devoria and Kamran Mohseni. On the mechanism of high-incidence lift generation for steadily translating low-aspect-ratio wings. *J. Fluid Mech.*, 813:110–126, 2017.

[69] Yuqi Huang, James Venning, Mark C. Thompson, and John Sheridan. Vortex separation and interaction in the wake of inclined trapezoidal plates. *J. Fluid Mech.*, 771:341–369, 2015.

[70] W. F. Phillips. Lifting-Line Analysis for Twisted Wings and Washout-Optimized Wings. *J. Aircr.*, 41(1):128–136, 2004.

[71] J Katz. A discrete vortex method for non-steady separted flow over an airfoil. *J. Fluid Mech.*, 102(315-328), 1981.

[72] H Babinsky, P R R J Stevens, A R Jones, L P Bernal, and M V Ol. Low Order Modelling of Lift Forces for Unsteady Pitching and Surging Wings . In *54th AIAA Aerosp. Sci. Meet. AIAA SciTech Forum, (AIAA 2016-0290)*, pages 1–12, 2016.

[73] P R R J Stevens, H Babinsky, F Manar, P Mancini, A R Jones, K O Granlund, T Nakata, N Phillips, R J Bomphrey, and A C Gozukara. Low Reynolds Number Acceleration of Flat Plate Wings at High Incidence (Invited). In *54th AIAA Aerosp. Sci. Meet. AIAA SciTech Forum, (AIAA 2016-0286)*, pages 1–15, 2016.

[74] Simon J. Corkery and Holger Babinsky. Force Production Mechanisms for a Flat Plate Wing at Low Reynolds Numbers. *2018 AIAA Aerosp. Sci. Meet.*, (January):1–13, 2018.

[75] Juhi Chowdhury and Matthew J. Ringuette. A simple vortex-loop-based model for unsteady rotating wings. *J. Fluid Mech.*, 880:1020–1035, 2019.

[76] F Noca, D Shiels, and Jeon D. A Comparison of Methods for Evaluating time-dependent fluid dynamic forces on bodies using only velocity fields and their derivatives. *J.\ Fluids Struct.*, 13:551–578, 1999.

[77] Jie Zhi Wu, Ze Liang Pan, and Xi Yun Lu. Unsteady fluid-dynamic force solely in terms of control-surface integral. *Phys. Fluids*, 17(9):1–4, 2005.

[78] J. Z. Wu, X. Y. Lu, and L. X. Zhuang. Integral force acting on a body due to local flow structures. *J. Fluid Mech.*, 576:265–286, 2007.

[79] L. L. Kang, L. Q. Liu, W. D. Su, and J. Z. Wu. Minimum-domain impulse theory for unsteady aerodynamic force. *Phys. Fluids*, 30(1), 2018.

[80] J M Burgers. On the resistance of fluid and vortex motion. In *Proc. K. Akad. Wet.*, volume 23, pages 774–782, 1920.

[81] J. C. Wu. Theory for Aerodynamic Force and Moment in Viscous Flows, 1981.

[82] J. Lighthill. *An informal introduction to theoretical fluid mechanics.* 1986.

[83] Jeff D Eldredge. *Mathematical Modeling of Unsteady Inviscid Flows*. Springer, 2019.

[84] P Koumoutsakos and A Leonard. High-resolution simulation of the flow around an impulsively started cylinder using vortex methods. *J. Fluid Mech.*, 296:1–38, 1995.

[85] A Leonard and A Roshko. Aspects of flow-induced vibrations. *J. Fluids Struct.*, 15:415–425, 2001.

[86] David Lentink. Accurate fluid force measurement based on control surface integration. *Exp. Fluids*, 59(1):1–12, 2018.

[87] David E. Rival and Bas van Oudheusden. Load-estimation techniques for unsteady incompressible flows. *Exp. Fluids*, 58(3):1–11, 2017.

[88] B. Protas. On calculation of hydrodynamic forces for steady flows in unbounded domains. *J. Fluids Struct.*, 27(8):1455–1460, 2011.

[89] B C Basu and G J Hancock. The unsteady motion of a two-dimensional aerofoil in incompressible inviscid flow. *Commun. Pure Appl. Math.*, 87(1):159–178, 1978.

[90] D. Kim and M. Gharib. Characteristics of vortex formation and thrust performance in drag-based paddling propulsion. *J. Exp. Biol.*, 214(13):2283–2291, 2011.

[91] Horace Lamb. *Hydrodynamics*. 1932.

[92] P. G. Saffman and J. S. Sheffield. Flow over a Wing with an Attached Free Vortex. *Stud. Appl. Math.*, 57(2), 1977.

[93] Ming-Ke Huang and Chuen-Yen Chow. Trapping of a free vortex by airfoils with surface suction. *AIAA J.*, 24(8):1217–1218, 1986.

[94] H. L. F. von Helmholtz. Über discontinuierliche Flüssigkeitsbewegungen. *Monatsberichte der Königlichen Akad. der Wissenschaften zu Berlin*, 23:215–228, 1868.

[95] H G von Kirchhoff. Zur Theorie freier Flüssigkeitsstrahlen. *J. für Math.*, LXX(4):289–298, 1868.

[96] F R S Lord Rayleigh. On the Resistance of Fluids. *Philos. Mag. J. Sci.*, 2(5):430–441, 1876.

[97] A Fage and F C Johansen. XLII. The structure of vortex sheets. *London, Edinburgh, Dublin Philos. Mag. J. Sci.*, 5(28):417–441, feb 1928.

[98] September ESDU. Fluid Forces and Moments on Flat Plates. Data Item 70015. *Eng. Sci. Data Unit, London, UK*, 1970.

[99] Jie Zhi Wu, Hui Yang Ma, and Ming De Zhou. *Vorticity and vortex dynamics*. 2006.

[100] L. M. Milne-Thomson. Theoretical Aerodynamics (4th Edition), 1958.

[101] L Prandtl. Königliche Gesellschaft der Wissenschaften zu Göttingen. *Tragflügeltheorie*, 1918.

[102] Frank M. White. *Fluid Mechanics, 7th Edition*. 2011.

[103] Joseph Katz and Allen Plotkin. *Low-Speed Aerodynamics*. 2001.

[104] C. W. Pitt Ford and H. Babinsky. Lift and the leading-edge vortex. *J. Fluid Mech.*, 720:280–313, 2013.

[105] S. J. Corkery, Holger Babinsky, and W. R. Graham. Quantification of added-mass effects using particle image velocimetry data for a translating and rotating flat plate. *J. Fluid Mech.*, 870:492–518, 2019.

[106] C P Ellington, C van den Berg, A P Willmott, and A L R Thomas. Leading edge vortices in insect flight. *Nature*, 384(19/26 December), 1996.

[107] J.M. M Birch and M.H. H Dickinson. No Title. *Nature*, 412(6848):729–733, 2001.

[108] F. T. Muijres, L. C. Johansson, R. Barfield, M. Wolf, G. R. Spedding, and A. Hedenstrom. Leading-Edge Vortex Improves Lift in Slow-Flying Bats. *Science (80- .)*., 319(5867):1250–1253, 2008.

[109] D. Lentink and M. H. Dickinson. Rotational accelerations stabilize leading edge vortices on revolving fly wings. *J. Exp. Biol.*, 212(16):2705–2719, 2009.

[110] D Lentink. Leading-Edge Vortices Elevate Lift of Autorotrating Plant Seeds. *Science (80-.).*, 1438(2009):10–13, 2011.

[111] J. J. Videler. Leading-Edge Vortex Lifts Swifts. *Science (80-.).*, 306(5703):1960–1962, 2004.

[112] R. R. Harbig, J. Sheridan, and M. C. Thompson. Reynolds number and aspect ratio effects on the leading-edge vortex for rotating insect wing planforms. *J. Fluid Mech.*, 730:52–75, 2013.

[113] Jaimea G. Wong and Davida E. Rival. Determining the relative stability of leading-edge vortices on nominally two-dimensional flapping profiles. *J. Fluid Mech.*, 766:611–625, 2015.

[114] Mostafa R.A. A. Nabawy and William J. Crowther. The role of the leading edge vortex in lift augmentation of steadily revolving wings: a change in perspective. *J. R. Soc. Interface*, 14(132):20170159, 2017.

[115] Thomas Linehan and Kamran Mohseni. On the maintenance of an attached leading-edge vortex via model bird alula, 2020.

[116] L W Bryan, D H Williams, and G I Taylor. An Investigation of the Flow of Air Around an Airfoil of Infinite Span. *Phil. Trans. R. Soc. Lond. A*, 225(626-635):199–245, 1925.

[117] L. Q. Liu, J. Z. Wu, W. D. Su, and L. L. Kang. Lift and drag in three-dimensional steady viscous and compressible flow. *Phys. Fluids*, 29(11), 2017.

7 AUTHORS BIOGRAPHY

Dr Ignazio Maria Viola is Reader (Associate Professor) at the School of Engineering of the University of Edinburgh and a Fellow of the Royal Institution of Naval Architects (RINA). His research is in applied fluid dynamics, and focuses on those conditions where the forces on immersed bodies are governed by vortex flow and can be controlled by fluid-structure interaction. He has written more than 150 scientific publications, including 40 journal articles. He has been awarded two RINA Medals of Distinction and one RINA Medal of Exceptional Merit. He is Editor-in-Chief of the Journal of Sailing Technology of the Society of Naval Architects and Marine Engineers (SNAME).

Dr A. Arredondo-Galeana is Research Associate in marine energy at the University of Edinburgh. He obtained his PhD in 2019 in sailing aerodynamics with his thesis *A Study of the Vortex Flows of Downwind Sails*, under the supervision of Dr Viola. Abel continues to work in this field and has published articles in the Journal of Sailing Technology and Ocean Engineering. He holds an MSc degree from the University of Edinburgh where he worked on the design of a self-damping Flettner rotor. His current interests include sail aerodynamics, particle image velocimetry, tidal energy and flow control.

G. Pisetta is a PhD candidate at the University of Edinburgh. His PhD thesis aims at the development of a potential flow model of a thin plate with variable camber, to understand the underlying fluid mechanics principles of unsteady load mitigation by shape-morphing. His previous experience includes the low order modelling of tidal turbine blades subjected to unsteady inflow conditions, and the performance analysis of tidal turbines equipped with morphing blades.